RECENT ADVANCES IN CONSTITUTIVE MODELLING OF COMPACTION OF GRANULAR MATERIALS UNDER CYCLIC LOADING

Torsten Wichtmann, Andrzej Niemunis, Theodor Triantafyllidis

Institute for Soil Mechanics and Rock Mechanics
University of Karlsruhe
Engler-Bunte-Ring 14, 76131 Karlsruhe, Germany
e-mail: torsten.wichtmann@ibf.uka.de, web page: http://www.ibf.uni-karlsruhe.de

Keywords: sand, cyclic loading, accumulation, high-cycle model, material constants, elastic stiffness

Abstract. *The paper briefly summarizes the high-cycle accumulation model recently proposed by the authors. The model predicts permanent deformations and / or excess pore water pressures in non-cohesive soils due to many cycles ($N > 10^3$) with relatively small amplitudes ($\varepsilon^{ampl} < 10^{-3}$, so-called high- or polycyclic loading). Correlations of the material constants of the model with index and granulometric properties are discussed. For this purpose the material constants of eight different grain size distribution curves of a quartz sand were determined in approx. 200 cyclic triaxial tests. The correlations may be utilized for a simplified procedure to determine a set of material constants. The "elastic" stiffness E in the basic equation $\dot{\sigma}' = \mathsf{E} : (\dot{\varepsilon} - \dot{\varepsilon}^{acc})$ of the model interrelates quasi-creep and quasi-relaxation. In order to develop a suitable E, the accumulation of pore water pressure in 15 undrained cyclic tests and the accumulation of volumetric strain in 15 drained cyclic tests with similar initial conditions were compared.*

1 INTRODUCTION

The high-cycle accumulation model recently proposed by the authors (Niemunis et al. [2]) predicts permanent deformations or excess pore water pressures in non-cohesive soils due to many cycles ($N > 10^3$) with relatively small amplitudes ($\varepsilon^{\mathrm{ampl}} < 10^{-3}$, so-called high- or polycyclic loading). It is based on an extensive laboratory testing program (Wichtmann et al. [6, 8–11]). An outline of the model is given in Section 2. Typically, the model can be applied to foundation systems subjected to traffic loading (e.g. high speed trains), to wind power plants (offshore and onshore), to machine foundations and to problems related to mechanical compaction of granular soils.

Up to present the determination of the material constants of the high-cycle model is laborious. At least 9 cyclic triaxial tests each with a duration of at least half a week (100,000 cycles at a frequency of 1 Hz) are necessary and sophisticated test devices are indispensable. In order to develop a simplified procedure we have investigated correlations between the material constants and the granulometric (e.g. mean grain diameter d_{50}, uniformity index C_u) or index properties (e.g. minimum void ratio $e_{\min}$). Till now approx. 200 cyclic triaxial tests were performed in order to determine the constants for eight sands with different grain size distribution curves. The number of tests was chosen larger than necessary in order to examine some dependencies more thoroughly. The test results, possible correlation formulas and a first approach for a simplified calibration procedure are presented in Section 3.

A major novel finding wrt [2] is a peculiar variability of the "elastic" stiffness E in the basic equation $\dot{\sigma}' = \mathsf{E} : (\dot{\varepsilon} - \dot{\varepsilon}^{\mathrm{acc}})$ of the model with the number of cycles N. E interrelates the quasi-creep $\dot{\varepsilon} = \dot{\varepsilon}^{\mathrm{acc}}$ and the quasi-relaxation $\dot{\sigma}' = -\mathsf{E} : \dot{\varepsilon}^{\mathrm{acc}}$. While the prescribed rate of strain accumulation $\dot{\varepsilon}^{\mathrm{acc}}$ was extensively studied in drained cyclic triaxial tests, relatively sparse information is available on E. In the boundary value problems (BVPs) which we have studied up to now the deformations (e.g. settlements of shallow foundations on dry sand, Wichtmann et al. [7]) were of essential importance and less attention was paid to an appropriate formulation of E, because the evolution of the stress rate (trend) $\dot{\sigma}$ was believed to be less significant. However, for some BVPs in which considerable changes of the average stress are expected, a closer inspection of E becomes necessary. It may be studied by comparing the quasi-creep (accumulation of residual strain) in drained cyclic tests and the quasi-relaxation of effective stress (accumulation of excess pore water pressure) in undrained cyclic tests. Such a comparison is undertaken in Section 4. The stiffness during re-consolidation (post-cyclic behaviour) is also addressed.

Further advances (e.g. ideas for a better tensorial definition of an amplitude for multiaxial loops) and open questions referring to the high-cyclic behaviour of soils are briefly addressed in Section 5.

2 HIGH-CYCLE MODEL

The basic assumption of the high-cycle model (Niemunis et al. [2]) recently proposed by the authors is that the strain path and the stress path that result from a cyclic loading can be decomposed into an oscillating part and

Influencing parameter	Function	Material constants	Reference quantities
Strain amplitude	$f_{\text{ampl}} = \min\left\{\left(\frac{\varepsilon^{\text{ampl}}}{\varepsilon^{\text{ampl}}_{\text{ref}}}\right)^2; 100\right\}$		$\varepsilon^{\text{ampl}}_{\text{ref}} = 10^{-4}$
Cyclic preloading	$\dot{f}_N = \dot{f}^A_N + \dot{f}^B_N$ $\dot{f}^A_N = C_{N1}C_{N2}\exp\left[-\frac{g^A}{C_{N1}\,f_{\text{ampl}}}\right]$ $\dot{f}^B_N = C_{N1}C_{N3}$	C_{N1}, C_{N2}, C_{N3}	
Average mean pressure	$f_p = \exp\left[-C_p\left(\frac{p^{\text{av}}}{p_{\text{ref}}} - 1\right)\right]$	C_p	$p_{\text{ref}} = p_{\text{atm}}$ = 100 kPa
Average stress ratio	$f_Y = \exp(C_Y\,\overline{Y}^{\text{av}})$	C_Y	
Void ratio	$f_e = \frac{(C_e - e)^2}{1+e}\,\frac{1+e_{\text{ref}}}{(C_e - e_{\text{ref}})^2}$	C_e	$e_{\text{ref}} = e_{\max}$

Table 1: Summary of the functions, material constants and reference quantities of the high-cycle model

a trend. The oscillating part is described by the strain amplitude. The model predicts the trend (accumulation) of strain $\dot{\varepsilon}^{\text{acc}}$ only. Depending on the boundary conditions, the trend of stress (pseudo-relaxation) or of strain (pseudo-creep) can be observed. They are interrelated by

$$\dot{\sigma}' = \mathsf{E} : (\dot{\varepsilon} - \dot{\varepsilon}^{\text{acc}} - \dot{\varepsilon}^{\text{pl}}) \tag{1}$$

with the stress rate $\dot{\sigma}'$ of the effective stress σ' (compression positive), the strain rate $\dot{\varepsilon}$ (compression positive), the given accumulation rate $\dot{\varepsilon}^{\text{acc}}$, a plastic strain rate $\dot{\varepsilon}^{\text{pl}}$ (for stress paths touching the yield surface) and the elastic stiffness E. In the context of high-cycle models "rate" means a derivative with respect to the number of cycles N (instead of time t), i.e. $\dot{\sqcup} = \partial \sqcup / \partial N$. The total stress is denoted by $\sigma = \sigma' + u\mathbf{1}$ with the pore water pressure u. For $\dot{\varepsilon}^{\text{acc}}$ in Eq. (1) we use

$$\dot{\varepsilon}^{\text{acc}} \quad = \quad \dot{\varepsilon}^{\text{acc}}\,\mathbf{m} \tag{2}$$

with the flow rule $\mathbf{m} = \dot{\varepsilon}^{\text{acc}}/\|\dot{\varepsilon}^{\text{acc}}\| = (\dot{\varepsilon}^{\text{acc}})^{\rightarrow}$ (unit tensor) and the flow intensity $\dot{\varepsilon}^{\text{acc}} = \|\dot{\varepsilon}^{\text{acc}}\|$. The superposed arrow denotes Euclidean normalization. Although the flow rule of the modified Cam clay (MCC) model

$$\mathbf{m} \quad = \quad \left[\frac{1}{3}\left(p - \frac{q^2}{M^2 p}\right)\mathbf{1} + \frac{3}{M^2}\sigma^*\right]^{\rightarrow} \tag{3}$$

significantly overestimates the Jaky's formula $K_0 = 1 - \sin\varphi$ for monotonic 1D compression, it approximates well the ratios $\dot{\varepsilon}^{\text{acc}}_v/\dot{\varepsilon}^{\text{acc}}_q$ measured in drained cyclic triaxial tests ($\dot{\varepsilon}_v$, $\dot{\varepsilon}_q$ = rates of volumetric or deviatoric strain, respectively). $\sqcup^*$ denotes the deviatoric part of $\sqcup$ and p,q are Roscoe's invariants. For the triaxial case $p = (\sigma'_1 + 2\sigma'_3)/3$ and $q = \sigma'_1 - \sigma'_3$ holds. For triaxial extension ($\eta = q/p < 0$) a small modification $M = F\,M_c$ is used with

$$F = \begin{cases} 1 + M_e/3 & \text{for } \eta \le M_e \\ 1 + \eta/3 & \text{for } M_e < \eta < 0 \\ 1 & \text{for } \eta \ge 0 \end{cases} \qquad \text{wherein} \quad M_c \;=\; \frac{6\sin\varphi_c}{3 - \sin\varphi_c} \quad \text{and} \quad M_e \;=\; -\frac{6\sin\varphi_c}{3 + \sin\varphi_c}. \tag{4}$$

The intensity of strain accumulation $\dot{\varepsilon}^{\text{acc}}$ in Eq. (2) is calculated as a product of six functions:

$$\dot{\varepsilon}^{\text{acc}} \quad = \quad f_{\text{ampl}}\;\dot{f}_N\;f_e\;f_p\;f_Y\;f_\pi \tag{5}$$

Each function (see Table 1) considers the influence of a different parameter. The function f_{ampl} describes the proportionality between $\dot{\varepsilon}^{\text{acc}}$ and the square of the strain amplitude $(\varepsilon^{\text{ampl}})^2$. The stress-dependence (increase of $\dot{\varepsilon}^{\text{acc}}$ with decreasing p^{av} and increasing η^{av} ($\overline{Y}^{\text{av}} \approx \eta^{\text{av}}/M_c$) is captured by the functions f_p and f_Y while f_e expresses the increase of the rate with the void ratio. The function $\dot{f}_N$ describes the dependence of $\dot{\varepsilon}^{\text{acc}}$ on cyclic preloading (historiotropy). For a detailed description of f_π (increase of the accumulation rate due to changes of polarization) see [2].

The model incorporates also a tensorial definition of the amplitude for multidimensional strain loops [2]. It counts the cycles weighting them with their amplitude, i.e. the "fatigue" loading can be quantified by

$$g^A = \int f_{\text{ampl}} \, \dot{f}_N^A \, \mathrm{d}N \tag{6}$$

This variable is used for the cyclic preloading (historiotropic variable) in $\dot{f}_N$.

3 CORRELATION OF MATERIAL CONSTANTS WITH THE GRANULOMETRIC PROPERTIES

3.1 Test device and tested material

Four similar cyclic triaxial devices with pneumatic loading systems were used for the present study. They are described in detail by Wichtmann [6]. Specimens (diameter d = 10 cm, height h = 20 cm) were prepared by the pluviation technique (Wichtmann [6]) and tested under water-saturated conditions. Axial deformations and volume changes were measured.

Eight grain size distribution curves (Fig. 1) of a quartz sand with sub-angular grain shape and a specific weight of ρ_s = 2.65 g/cm^3 were tested. Up to present the high-cycle model was developed using test results for Sand No. 3. The mean grain diameters d_{50}, uniformity indices $C_u = d_{60}/d_{10}$, curvature indices $C_c = d_{30}^2/(d_{10}d_{60})$, maximum and minimum void ratios $e_{\max}$ and $e_{\min}$ (determined according to DIN 18126) and critical friction angles φ_c (obtained from cone pluviation tests) are summarized in Table 2.

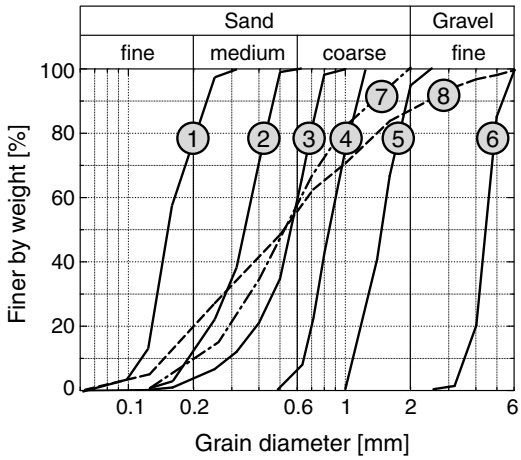

Figure 1: *Eight tested grain size distribution curves*

Sand No.	1	2	3	4	5	6	7	8
d_{50}[mm]	0.15	0.35	0.55	0.84	1.45	4.4	0.55	0.52
$C_u = d_{60}/d_{10}$	1.4	1.9	1.8	1.4	1.4	1.3	3.2	4.5
$C_c = d_{30}^2/(d_{10}d_{60})$	0.9	1.2	1.2	1.0	0.9	1.1	1.1	0.7
$e_{\max}$	0.992	0.930	0.874	0.878	0.886	0.851	0.811	0.691
$e_{\min}$	0.679	0.630	0.577	0.590	0.623	0.669	0.456	0.422
φ_c [°]	32.0	32.7	31.2	32.9	33.2	37.2	33.1	34.2

Table 2: Mean grain diameters d_{50}, uniformity indices C_u, curvature indices C_c, void ratios in loosest ($e_{\max}$) and densest ($e_{\min}$) condition and critical friction angles φ_c of the 8 tested sands

3.2 Test results: Direction of strain accumulation

For each sand four test series were performed. Throughout the tests of each series one parameter (stress amplitude, average mean pressure p^{av}, average stress ratio η^{av} or initial void ratio e_0) was varied while the other ones were kept constant. 100,000 cycles with a frequency of 1 Hz were applied in all tests.

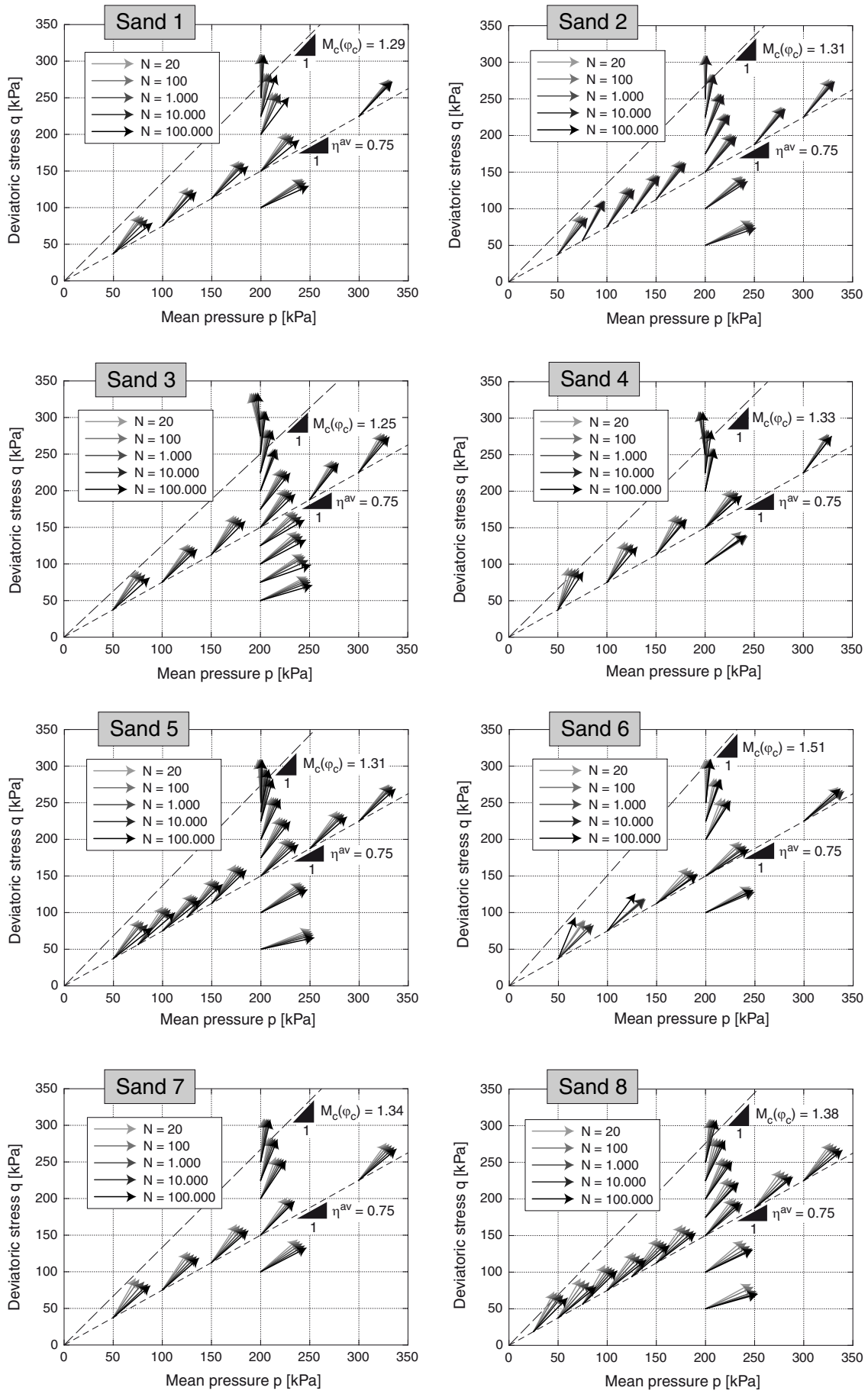

Figure 2: *Direction of strain accumulation shown as vectors in the p-q-plane*

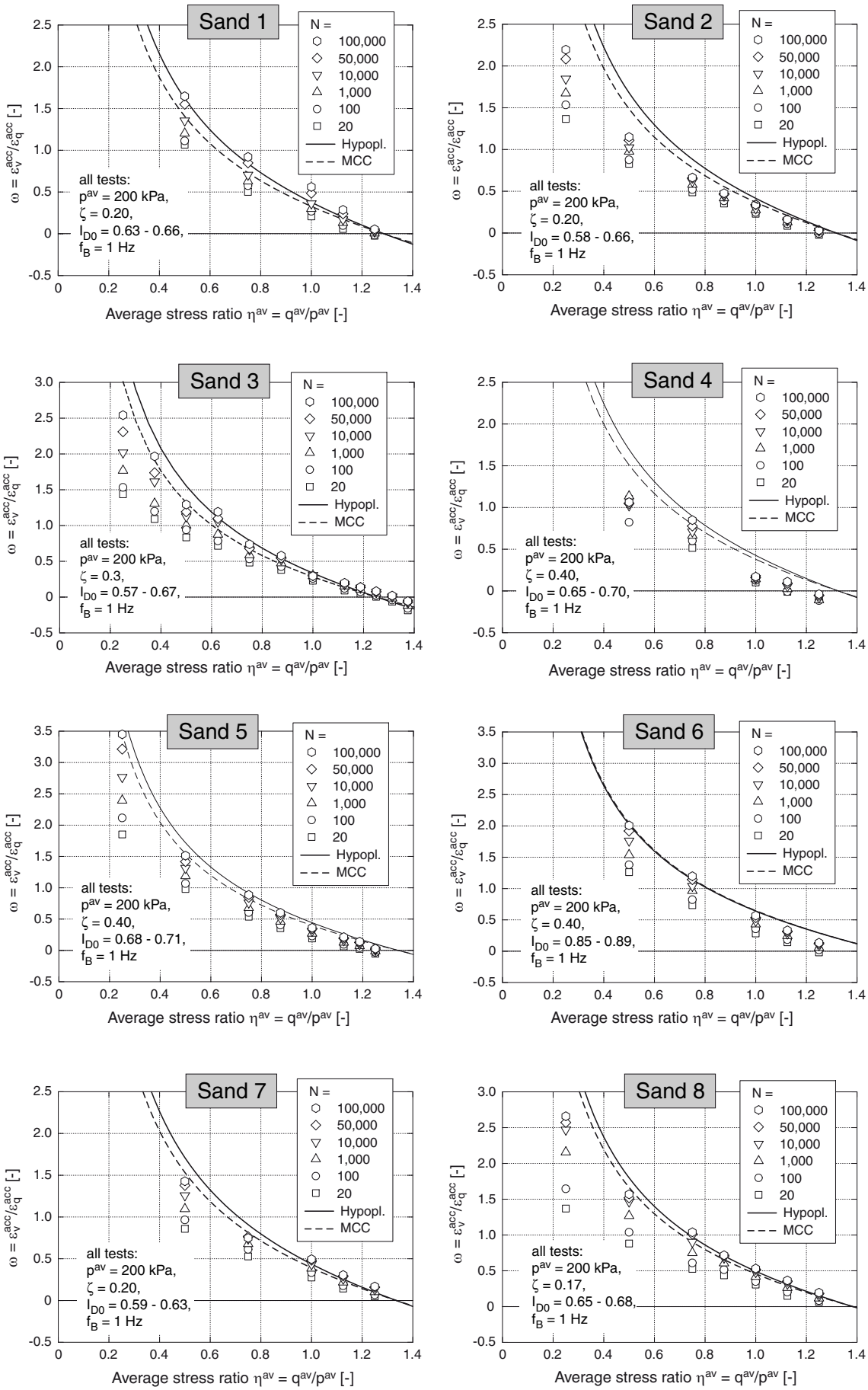

Figure 3: *Ratio* $\varepsilon_v^{acc}/\varepsilon_q^{acc}$ *as a function of average stress ratio* η^{av}

Relative density is expressed by the index $I_D = (e_{\max} - e)/(e_{\max} - e_{\min})$ and its initial value prior to cyclic loading is denoted by I_{D0}. The "irregular" first cycle is excluded from the diagrams since it is not described by the high-cycle model, i.e. $N = 1$ means after the first "regular" cycle.

For all eight sands the tests confirmed that the "cyclic flow rule" $\dot{\varepsilon}_v^{\mathrm{acc}}/\dot{\varepsilon}_q^{\mathrm{acc}}$ does neither depend on the stress amplitude nor on void ratio or average mean pressure. Neglecting a small influence of the number of cycles, **m** mainly depends on the average stress ratio $\eta^{\mathrm{av}} = q^{\mathrm{av}}/p^{\mathrm{av}}$. This may be concluded from Fig. 2 in which the direction of strain accumulation is presented as a vector in the p-q-plane with the inclination $\dot{\varepsilon}_q^{\mathrm{acc}}/\dot{\varepsilon}_v^{\mathrm{acc}}$ towards the horizontal and with the starting point at σ^{av}. For an isotropic stress a pure volumetric accumulation takes place and on the critical state line (CSL) it is approximately pure deviatoric. In Fig. 3 the ratio $\varepsilon_v^{\mathrm{acc}}/\varepsilon_q^{\mathrm{acc}}$ is plotted versus η^{av}. The flow rules of MCC and of the hypoplastic model fit well the experimental data, especially for large numbers of cycles. **The MCC flow rule may be used for all eight sands**.

3.3 Test results: Intensity of strain accumulation and correlation of material constants with granulometric properties

The test results confirmed findings in [6] that the accumulation rate $\dot{\varepsilon}^{\mathrm{acc}}$ increases with decreasing mean grain diameter d_{50} and increasing uniformity coefficient C_u.

Figure 4 presents the results of tests with different stress amplitudes q^{ampl}. The residual strain $\varepsilon^{\mathrm{acc}}$ after different numbers of cycles has been plotted versus the square of the strain amplitude $(\bar{\varepsilon}^{\mathrm{ampl}})^2$. The bar $\bar{\square}$ indicates that a mean value of the strain amplitude over N was used, because in the stress-controlled tests the strain amplitude may slightly vary. The residual strain has been normalized by the void ratio function f_e (which was calculated with a mean value of the void ratio over N) in order to consider slightly varying initial void ratios and different compaction rates. The linear curves in Fig. 4 confirm the square dependence of $\dot{\varepsilon}^{\mathrm{acc}}$ on $\varepsilon^{\mathrm{ampl}}$. **The function f_{ampl} is valid for all eight sands**.

Figure 5 contains the results of tests with different initial void ratios. In order to free the data from the influence of slightly different strain amplitudes the accumulated strain $\varepsilon^{\mathrm{acc}}$ has been divided by the amplitude function f_{ampl} and plotted versus a mean value of void ratio $\bar{e}$. The function f_e was fitted to the data for six different values of N. Mean values of the constant C_e are summarized in Table 3.

Figures 6 and 7 present the tests on the stress dependence. A fitting of functions f_p and f_Y delivers the material constants C_p and C_Y. Unfortunately, as already observed for Sand No. 3 these parameters turn out to vary slightly with N. In Table 3 we present just the mean values.

In Figure 8 the accumulation curves $\varepsilon^{\mathrm{acc}}(N)$ were normalized by the functions f_{ampl}, f_e, f_p and f_Y. A fitting of data with function $f_N = C_{N1}[\ln(1 + C_{N2}N) + C_{N3}N]$ delivered the constants C_{N1}, C_{N2} and C_{N3} given in Table 3. In the case of sand No. 4 the shape of the curves $\varepsilon^{\mathrm{acc}}(N)$ in the tests with q^{ampl} = 80 kPa at large stress ratios $\eta^{\mathrm{av}} > 1$ differs from the shape of the other curves. These curves are shown in Fig. 8 but have been neglected in the curve-fitting.

Constant	Sand							
	1	2	3	4	5	6	7	8
C_e	0.57	0.55	0.54	0.56	0.54	0.38	0.44	0.36
e_{ref}	0.992	0.930	0.874	0.878	0.886	0.851	0.811	0.691
C_p	0.60	0.84	0.43	0.58	0.68	0.30	0.68	0.61
p_{ref}	100 kPa	100 kPa	100 kPa	100 kPa	100 kPa	100 kPa	100 kPa	100 kPa
C_Y	1.8	2.7	2.0	2.8	2.8	3.0	2.2	3.1
C_{N1}	0.00087	0.00077	0.00036	0.00027	0.00043	0.000048	0.0044	0.0083
C_{N2}	0.22	0.27	0.43	0.38	0.32	1.27	0.029	0.0059
C_{N3}	0.00004	$7.4 \cdot 10^{-6}$	0.00005	0.00004	$7.0 \cdot 10^{-7}$	0	0.00005	0.00007

Table 3: Constants of the accumulation model for the eight tested sands

Fig. 9a presents the constant C_e as a function of $e_{\min}$. The correlation

$$C_e = 0.89\, e_{\min} \tag{7}$$

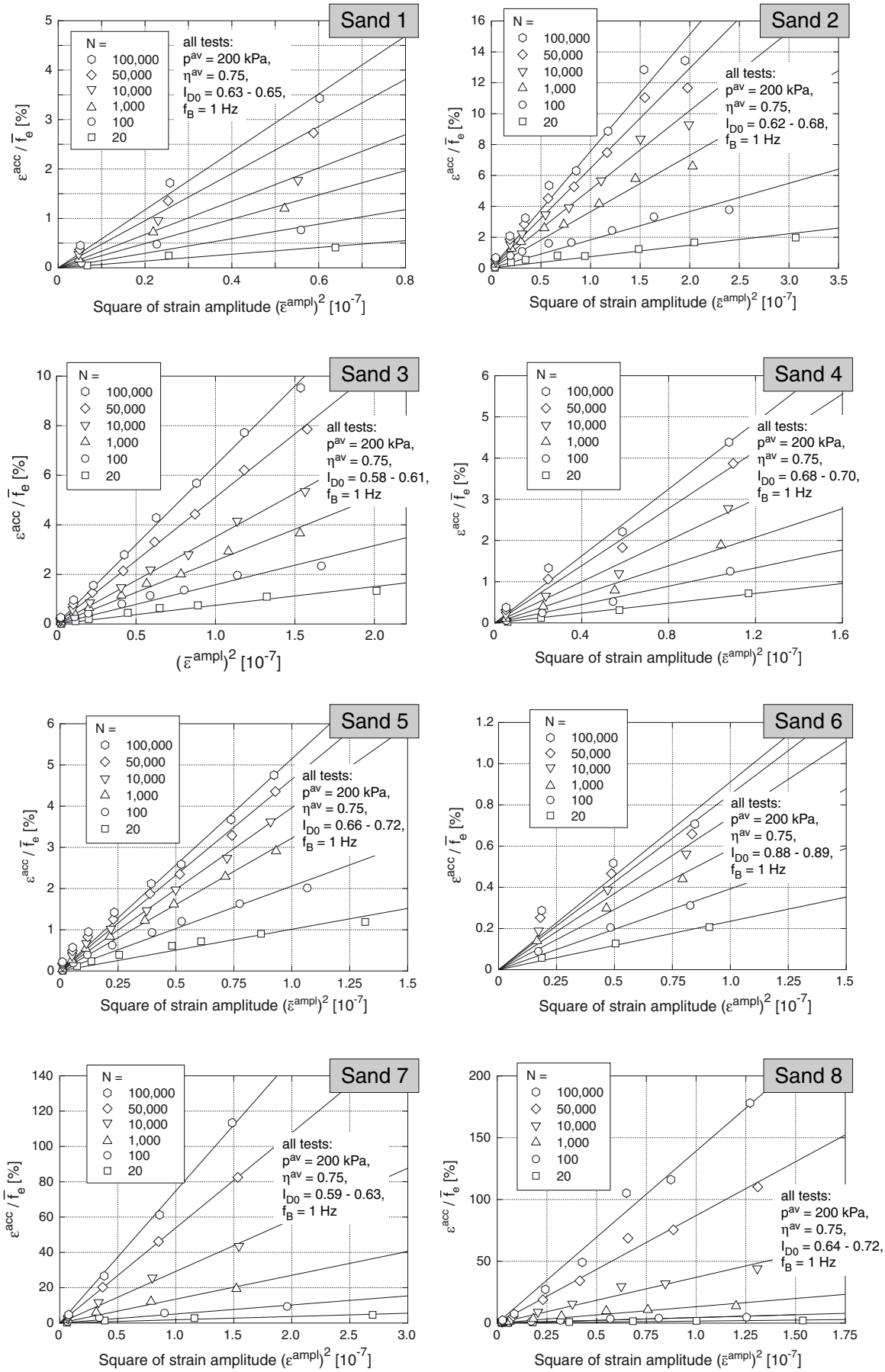

Figure 4: *Confi rmation of function f_{ampl} for the eight sands*

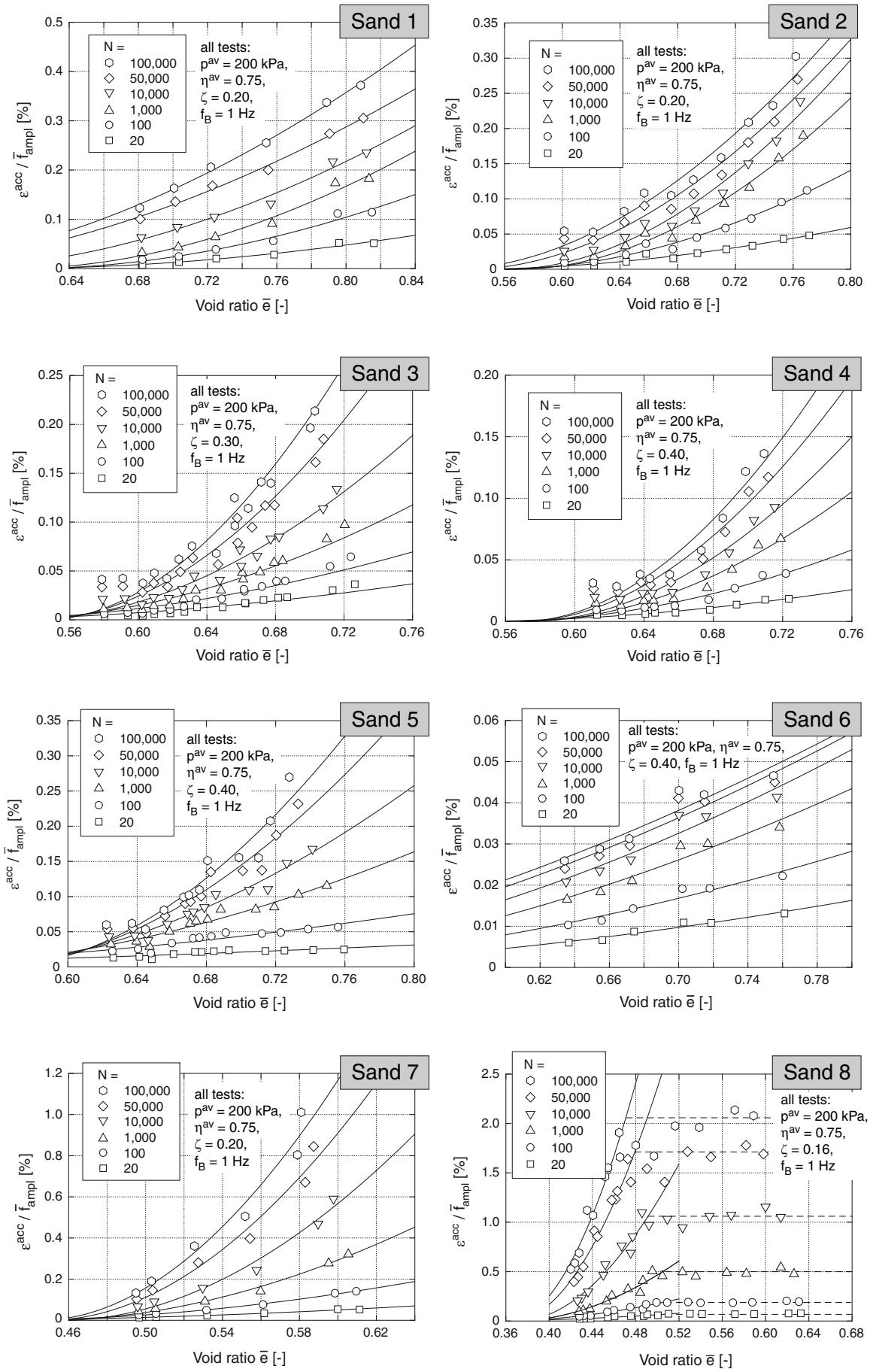

Figure 5: *Dependence* $\dot{\varepsilon}^{acc}(e)$*, fitting of function* f_e

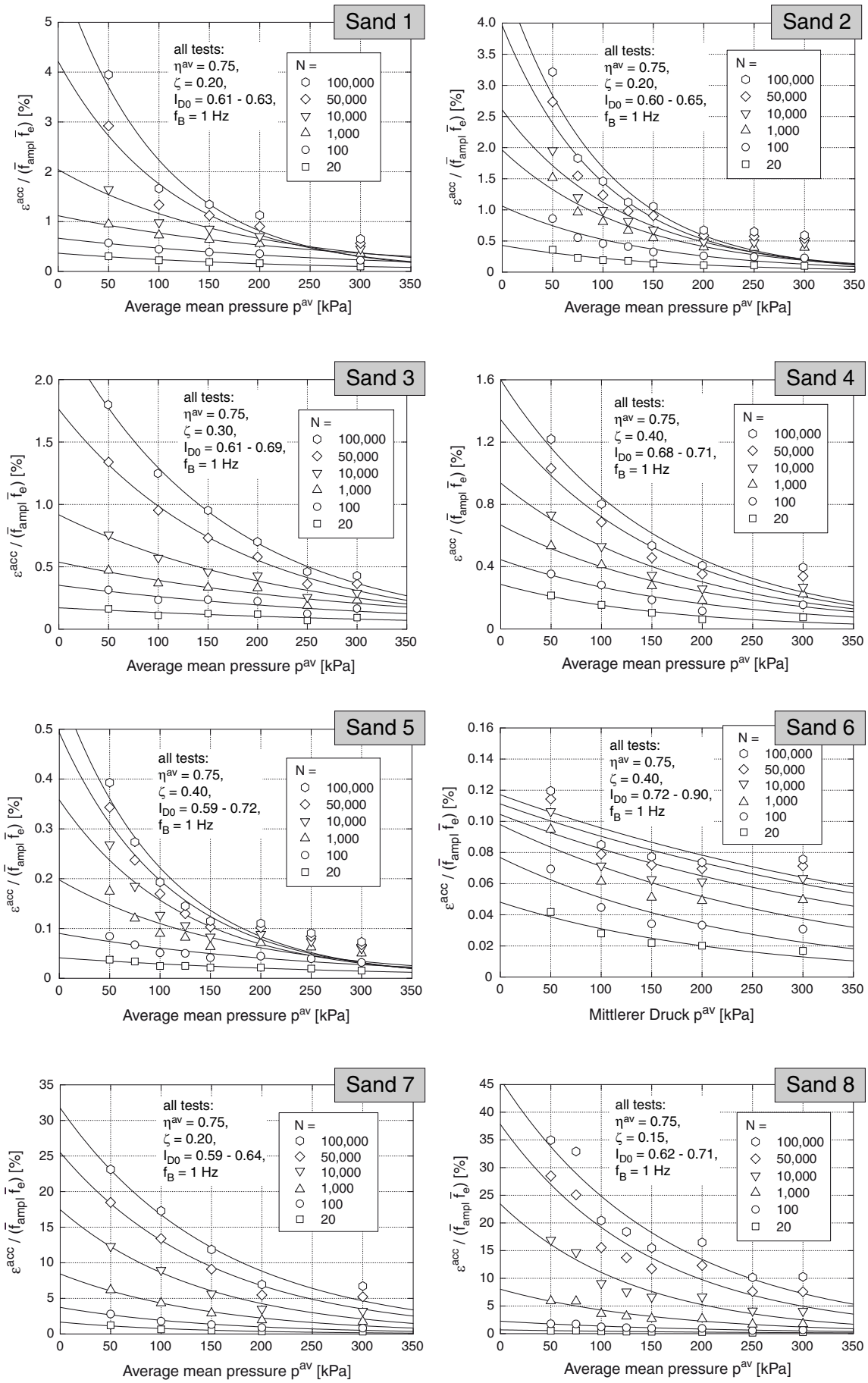

Figure 6: *Dependence* $\dot{\varepsilon}^{acc}(p^{av})$, *fitting of function* f_p

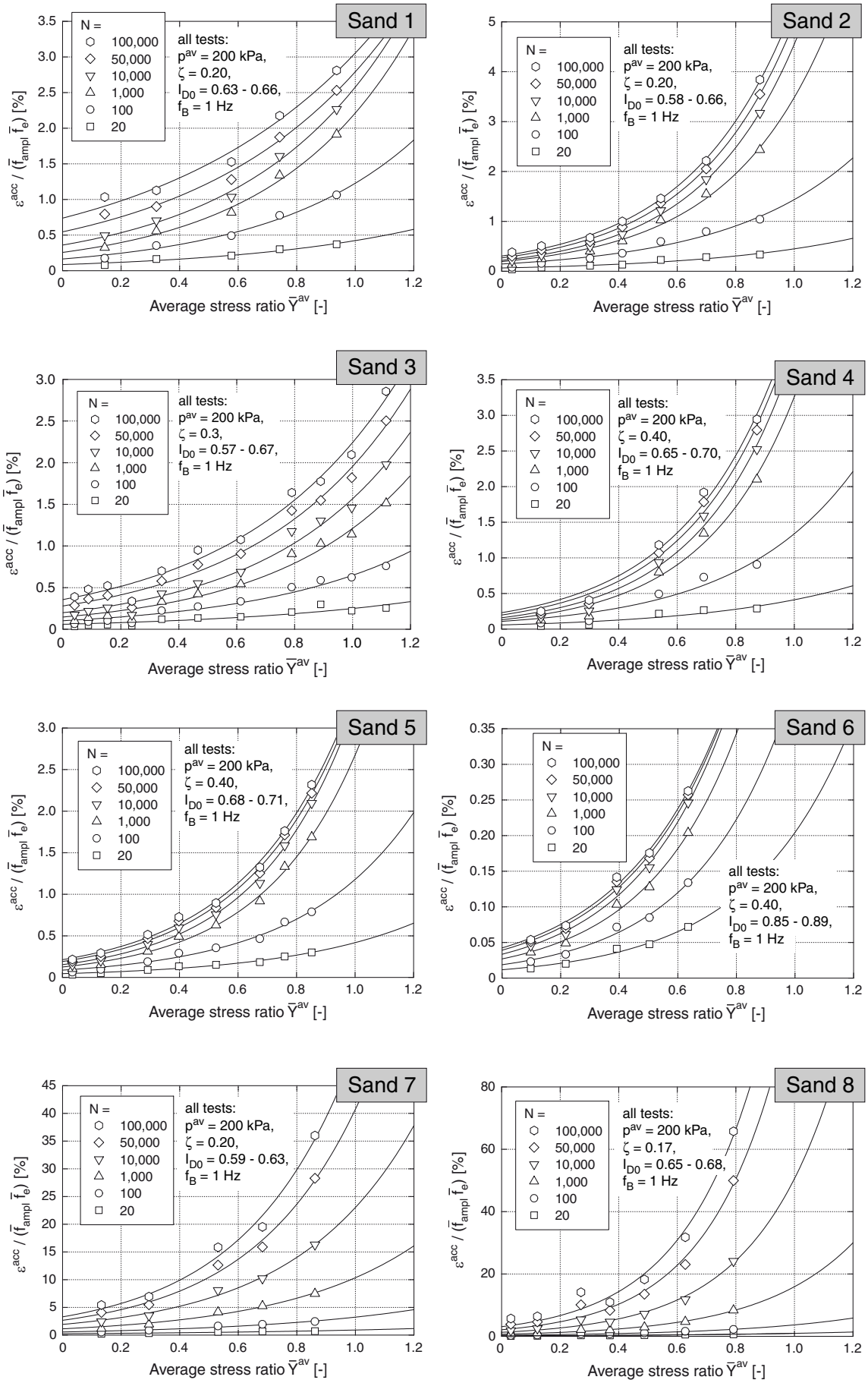

Figure 7: *Dependence* $\dot{\varepsilon}^{acc}(\overline{Y}^{av})$, *fitting of function* f_Y

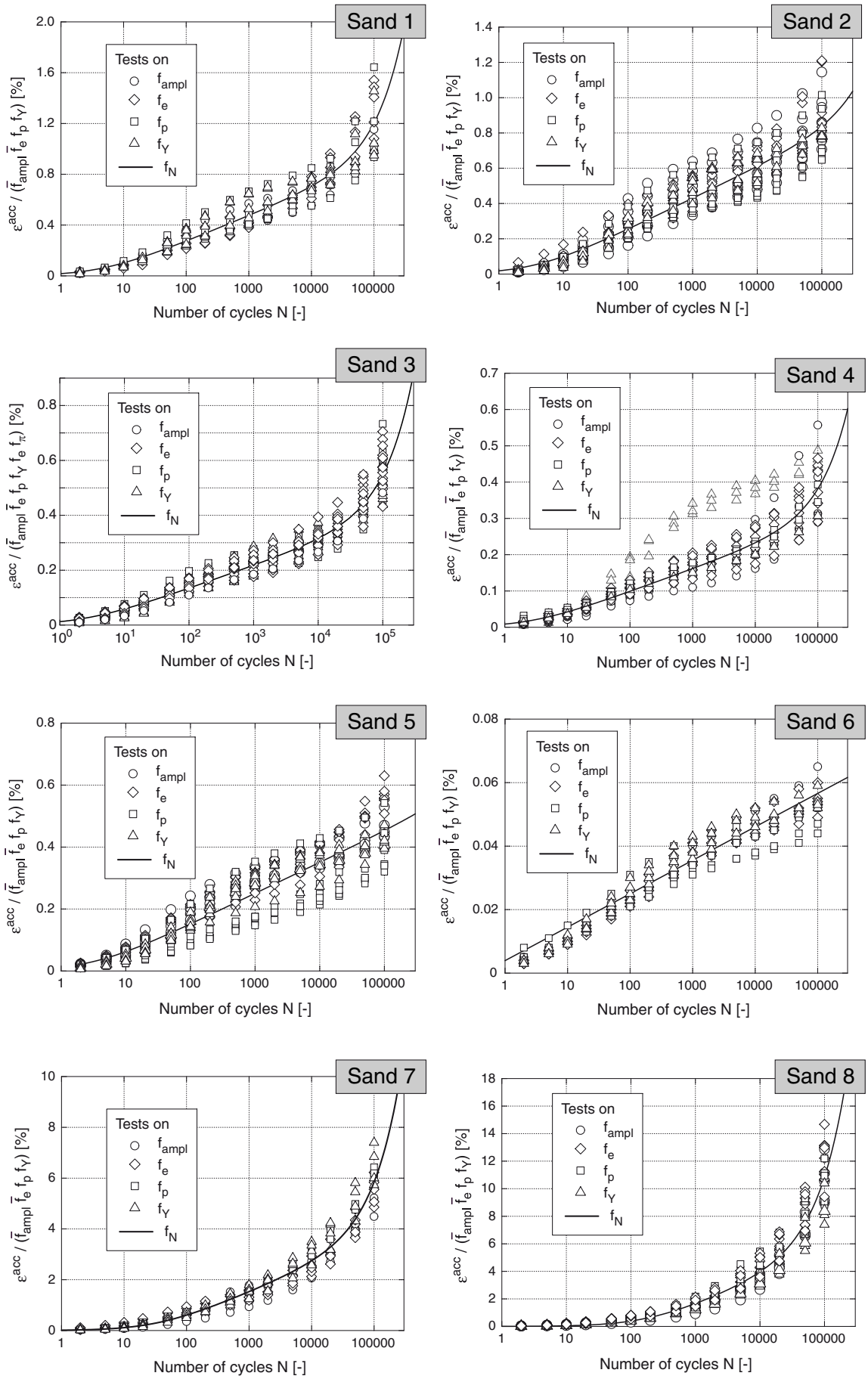

Figure 8: *Curves* $\varepsilon^{acc}/(\bar{f}_{ampl}\bar{f}_e f_p f_Y(N))$, *fitting of function* f_N

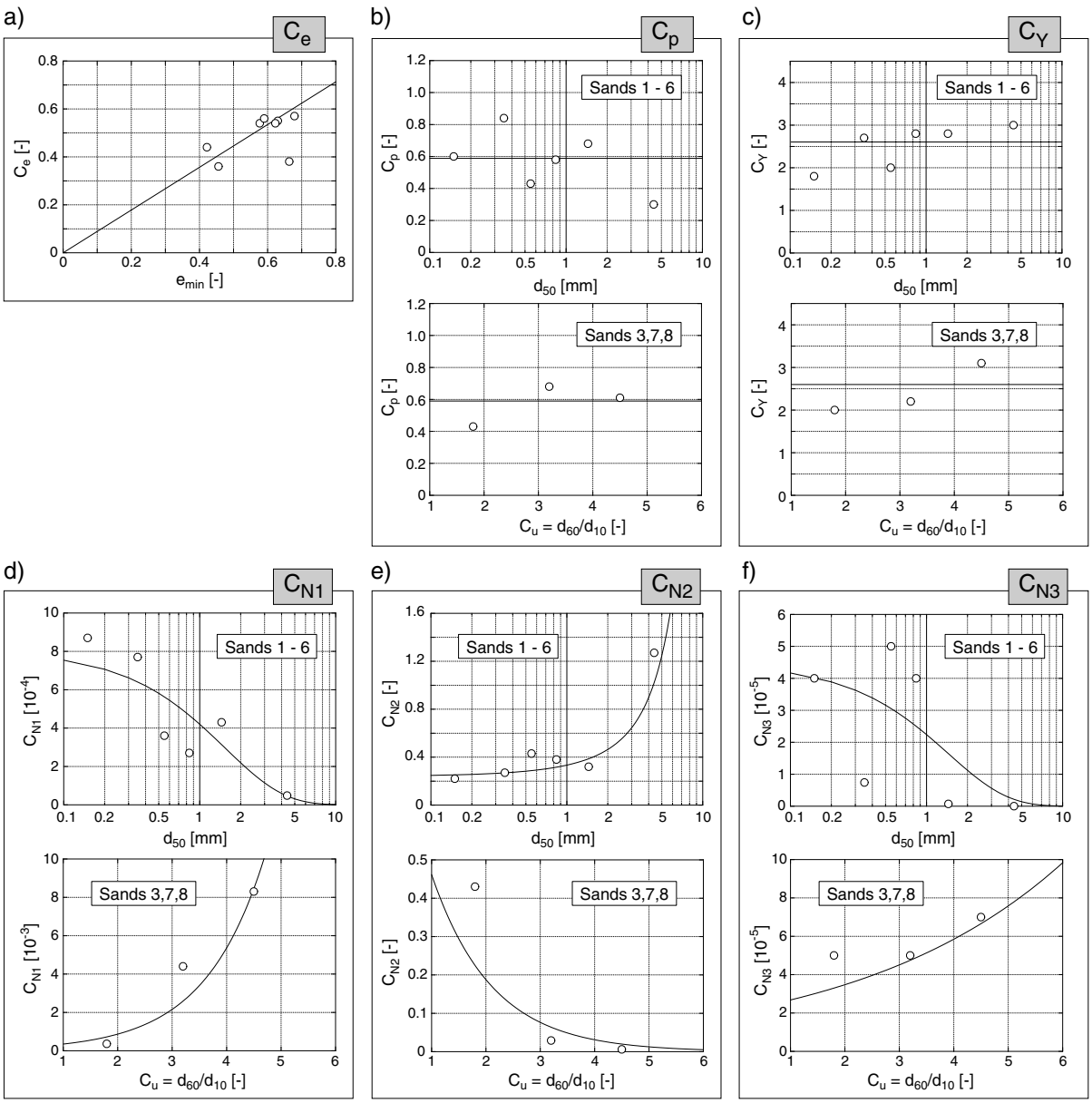

Figure 9: *Correlation of constant C_e with $e_{\min}$ and correlations of constants C_p, C_Y, C_{N1}, C_{N2} and C_{N3} with d_{50} and C_u*

approximates well the data except for the fine gravel No. 6. The independence of C_p and C_Y of d_{50} and C_u is shown in Fig. 9b and 9c. Although linear de- or increasing functions could be justified, the choice of constant values

$$C_p = 0.59 \quad \text{and} \quad C_Y = 2.6 \tag{8}$$

is recommended at present due to the few data points. The empirical correlation of C_{N1}, C_{N2} and C_{N3} with d_{50} and C_u (Fig. 9d-f) may be described by:

$$C_{N1} = 0.0002 \exp(-0.65\, d_{50}) \exp(0.91\, C_u) \tag{9}$$

$$C_{N2} = 0.95 \exp(0.33\, d_{50}) \exp(-0.90\, C_u) \tag{10}$$

$$C_{N3} = 0.00003 \exp(-0.69\, d_{50}) \exp(0.26\, C_u) \tag{11}$$

The data of C_{N3} show a significant scatter. C_{N3} dictates the accumulation at large N and may be better determined from tests with larger numbers of cycles $N > 10^5$. Such tests are planned in future.

A set of constants may be roughly estimated from Eqs. (7) to (11). If cyclic triaxial devices are available, a set of constants may be obtained with little effort by estimating C_e, C_p and C_Y from Eqs. (7) to (8) and by performing only one test in order to fit the constants C_{N1} to C_{N3}.

4 ”ELASTIC” STIFFNESS

The components of the isotropic stiffness tensor E have been formulated by comparing the rates of volumetric strain $\dot{\varepsilon}_v^{\mathrm{acc}}$ in 15 drained cyclic triaxial tests and the rates of pore water pressure $\dot{u}$ in 15 undrained cyclic tests. In all 30 tests the consolidation pressure prior to the drained or undrained cyclic loading was isotropic and the initial relative density was $I_{D0} \approx 0.60$. Five different initial pressures (p_0 = 50, 100, 150, 200 and 300 kPa) and three different amplitude ratios ($\zeta = q^{\mathrm{ampl}}/p_0$ = 0.2, 0.3 and 0.4) were tested.

The stress paths in the undrained tests are plotted in the p-q-plane in Fig. 10. Some of the tests were stopped when a certain amount of excess pore water pressure was reached, i.e. when the stress was still far away from the critical state line (CSL). In other tests the undrained cyclic loading was continued until the stress path reached the CSL or even until $\sigma' = \mathbf{0}$. The left side of Fig. 11 presents the trend of the pore water pressure $u(N)$. The right side of Fig. 11 contains diagrams with the curves $\varepsilon_v^{\mathrm{acc}}(N)$ of the drained tests.

The bulk modulus was calculated from $K = \dot{u}/\dot{\varepsilon}_v^{\mathrm{acc}}$ where $\dot{u}$ of an undrained test was divided by $\dot{\varepsilon}_v^{\mathrm{acc}}$ from the corresponding drained test (i.e. with same p_0 and q^{ampl}). In the undrained test, p^{av} evolves and the strain amplitude increases considerably with decreasing effective stress. In the drained test we have p^{av} = constant and the strain amplitude does not change much, but the void ratio e decreases with N. Thus, the rate $\dot{\varepsilon}_v^{\mathrm{acc}}$ was multiplied by four correction factors $f_{\mathrm{ampl}}^{UD}/f_{\mathrm{ampl}}^{D}$, f_e^{UD}/f_e^{D}, f_p^{UD}/f_p^{D} and $\dot{f}_N^{UD}/\dot{f}_N^{D}$ with the functions given in Table 1. The indices $\sqcup^{UD}$ and $\sqcup^{D}$ indicate the undrained or drained test, respectively. Because of the slow pore pressure accumulation, larger increments ΔN were chosen for the analysis of the tests with smaller amplitude ratios ζ. Data for which one of the correction factors would be larger than 2.0 or for which the strain amplitude would exceed $\varepsilon^{\mathrm{ampl}} = 10^{-3}$ are not considered in Fig. 12a-c. The bulk modulus K is presented versus p for the different values of ζ and for different numbers of cycles.

The bulk modulus during the first cycle (Fig. 12d) does not depend on the amplitude ratio ζ. Its increase with p can be approximated by

$$K \quad = \quad A\, p_{\mathrm{atm}}^{1-n}\, p^n \tag{12}$$

with constants A = 542 and n = 0.31. Interestingly, for all pairs of drained and undrained tests, K decreases with increasing number of cycles N (Fig. 12a-c and Fig. 12e). In Fig. 12e the correction for the dependence $K(p)$ has been made so that the figure shows the pure N-dependence. The reasons for the decrease of K with N are not well understood at present and need further investigation. A similar degradation of K was reported by Andersen during the post-cyclic behaviour of Drammen clay [1].

Most specimens were re-consolidated after undrained cyclic loading to p_0, q_0 and volume changes during this re-consolidation were measured. In Fig. 12f the bulk modulus $K = \Delta u/\Delta\varepsilon_v^{\mathrm{recons}}$ was plotted versus $p = p_0 - \Delta u/2$. The data from Fig. 12d and from a test with oedometric compression ($I_{D0} = 0.63$) was added to Fig. 12f. The oedometric K was estimated from the constrained elastic modulus M with the assumption ν = 0.2. The data includes curves for first loading, unloading and reloading. All three bulk moduli, from the first cycle, from re-consolidation and from oedometric reloading coincide. Only one data point from a test where the stress had reached $\sigma = \mathbf{0}$ lies lower than the rest. Such an unexpected large volume change during re-consolidation after undrained cycles near $\sigma = \mathbf{0}$ has already been reported by Niemunis et al. [3].

Until the decrease of K with N is better understood, it is recommended to use an isotropic E with K according to Eq. (12) and with $\nu = 0.2$.

5 SOME OTHER ADVANCES AND OPEN QUESTIONS

New ideas for a better definition of the amplitude for complex 6-dimensional strain loops were discussed by Niemunis et al. [4]. The amplitude is obtained by means of a spectral analysis assuming that the natural cyclic loading consists of 6-D harmonic oscillations distinguished by frequency.

Niemunis et al. [5] confronted a numerical and an experimental investigation on spatial stress fluctuations in the soil. While calculations with the accumulation model exhibited a smoothing of the initial field of stress fluctuations no correlation of cyclic preloading with acoustic emissions could be detected in the experiments with a model foundation. Unfortunately, we could not correlate the cyclic preloading variable g^A of the model with acoustic emissions.

Beside the somewhat surprising N-dependence of K reported in Section 4, some other open questions concerning the high-cyclic behaviour of granular soils remain. The accumulation at very large cycles $N > 10^6$ has not been

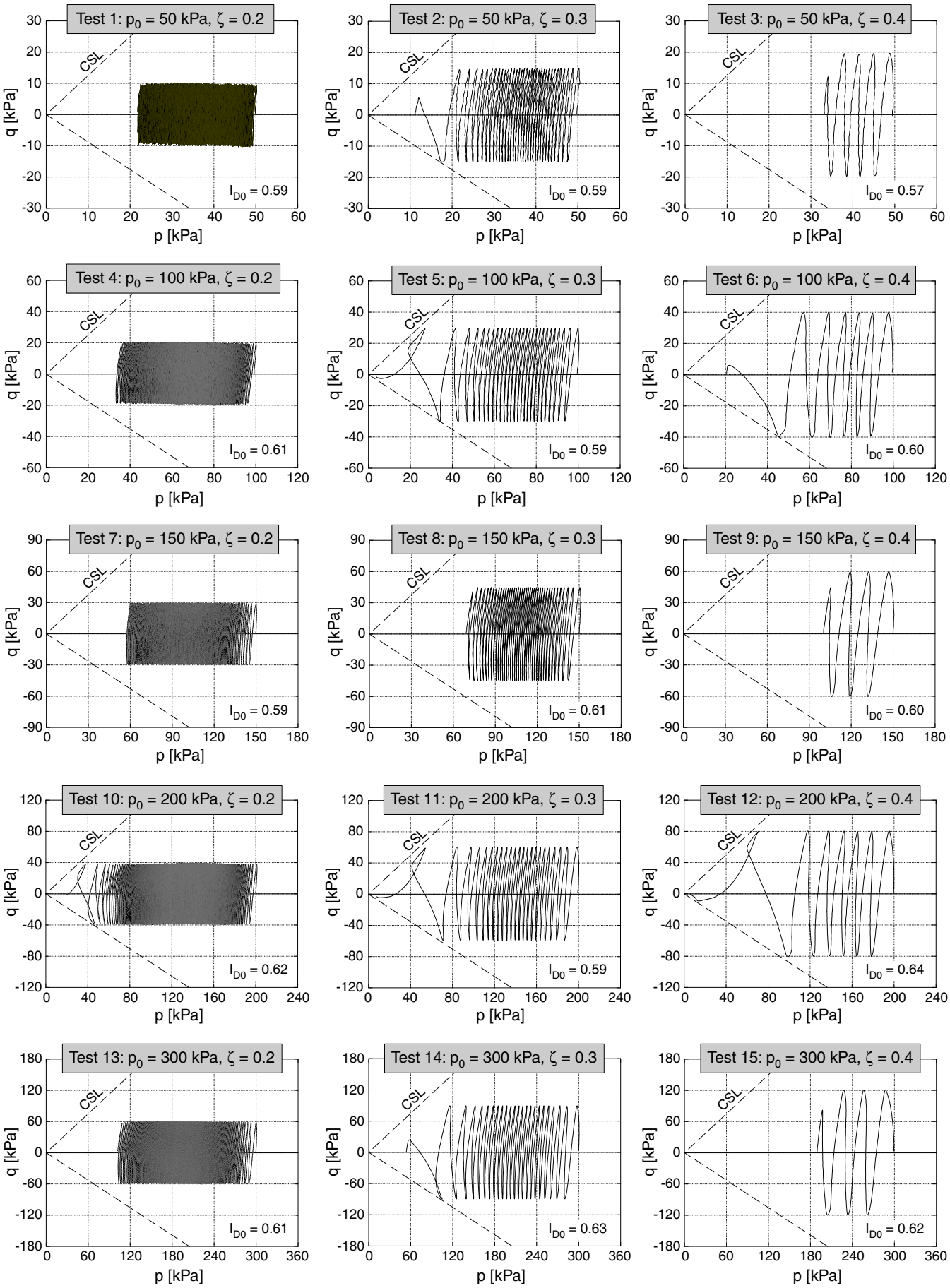

Figure 10: *Stress paths in the p-q-plane during the undrained cyclic tests*

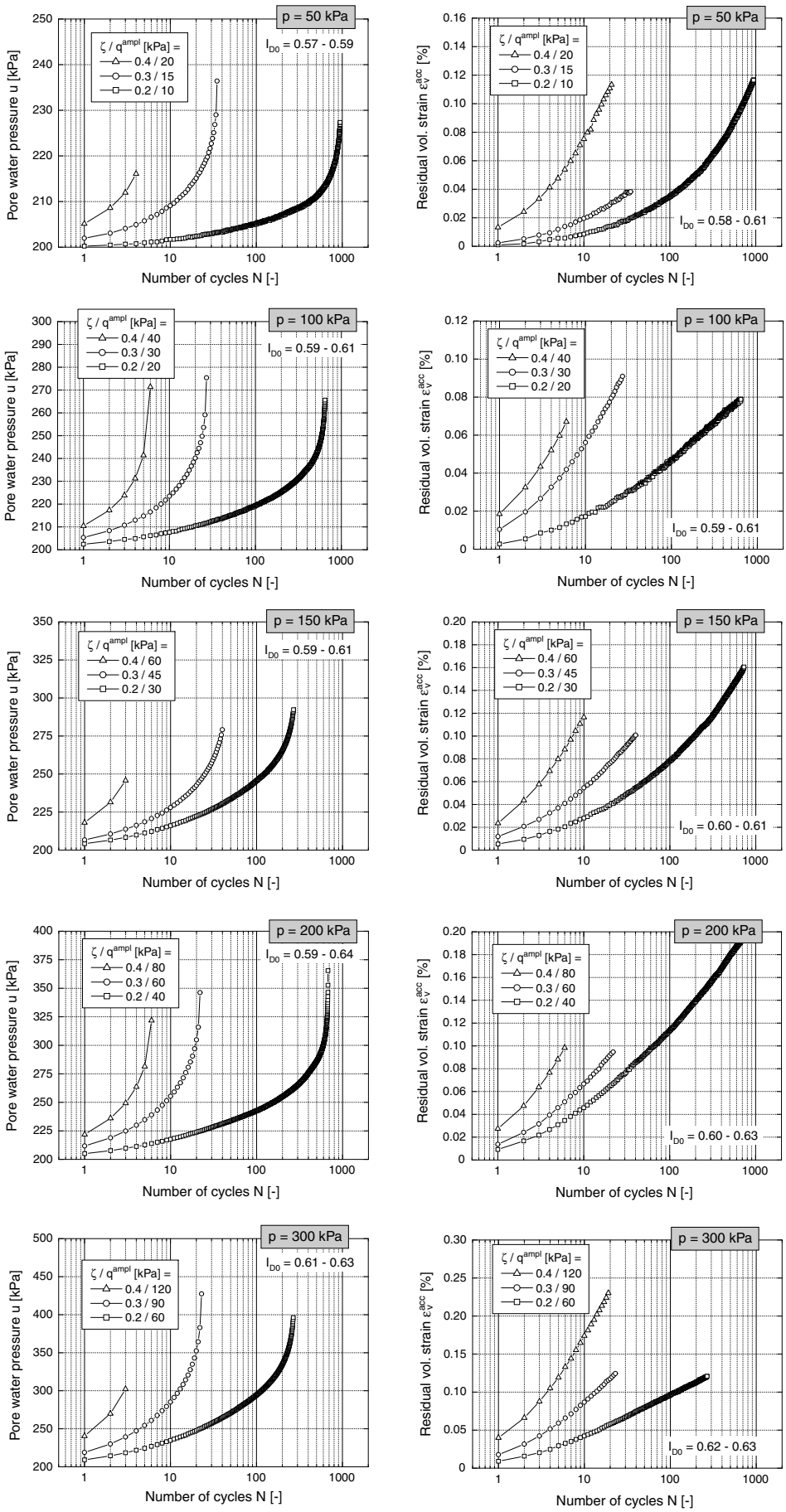

Figure 11: *Left: Accumulation of excess pore water pressure* $\Delta u(N)$ *in the undrained tests; Right: Accumulation of volumetric strain* $\varepsilon_v^{acc}(N)$ *in the drained tests*

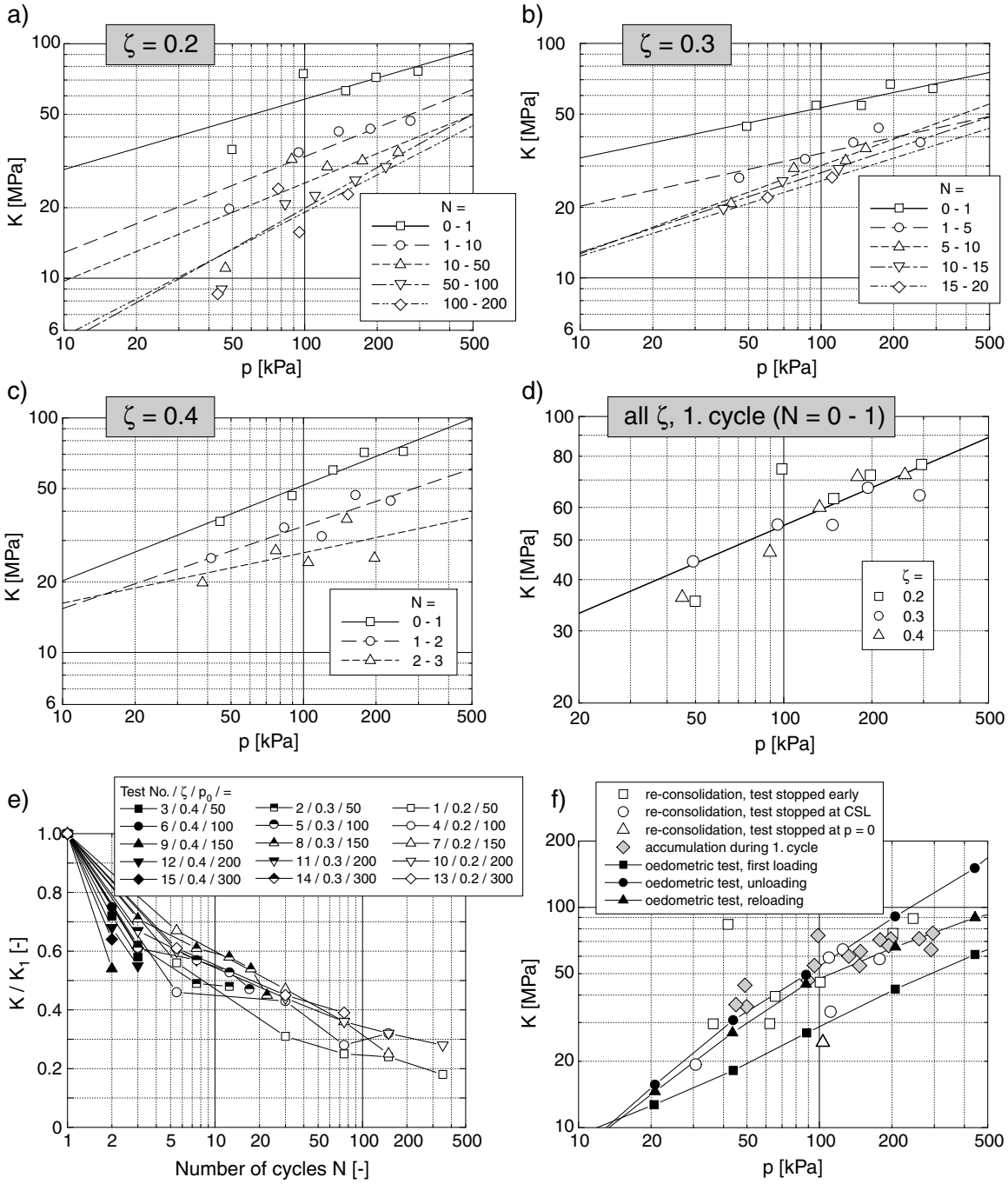

Figure 12: *a-d) Bulk modulus* $K = \dot{u}/\dot{\varepsilon}_v^{acc}$ *for different amplitude ratios* $\zeta = q^{ampl}/p_0$ *and numbers of cycles N, e) Bulk modulus K versus number of cycles N, f) Comparison of bulk moduli K from the first cycle, from re-consolidation and from an odeometric test*

investigated yet. Furthermore, the flow rule seems to be influenced by a cyclic preloading at a different σ^{av} as shown in Fig. 13. These topics will be further investigated in our laboratory.

6 SUMMARY AND CONCLUSIONS

Based on approx. 200 cyclic triaxial tests on eight different grain size distribution curves of a quartz sand a simplified procedure for the determination of the material constants of the high-cycle accumulation model is proposed. A closer examination of some elements of the model reveals some discrepancies between the model and the test results. However, an improvement of the prediction of the model seems possible at the cost of considerable complication of the constitutive equations. In particular, comparing the pore water pressure accumulation in undrained

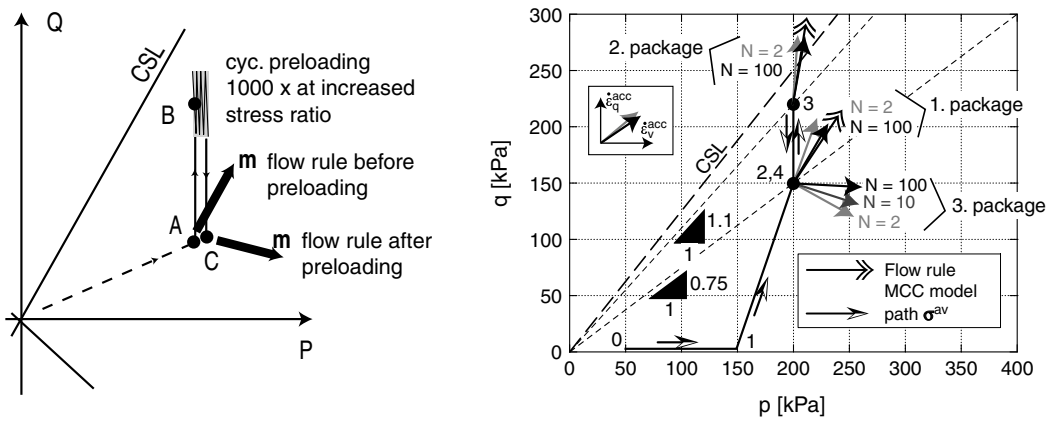

Figure 13: *Cyclic preloading at an increased stress ratio affects the rate and the direction of accumulation. This effect has not been included in the model as yet. Left: the idea of the test; Right: test results*

cyclic tests and the accumulation of volumetric strain in drained cyclic tests the stiffness E of the model was studied. It has been shown that the bulk modulus K during the first cycle is similar to the values of K during oedometric reloading and during re-consolidation. A decrease of K with N has to be further investigated in future.

ACKNOWLEDGEMENT

The authors are indepted to German Research Council (DFG) and the Federal Ministry for the Environment, Natural Conservation and Nuclear Savety (BMU) for the financial support within the Collaborate Research Centre SFB 398 ”Lifetime oriented design concepts” (project A8) or the project ”Geotechnical robustness and self-healing of foundations of offshore wind power plants”, respectively.

References

[1] K.H. Andersen, J.H. Pool, S.F. Brown, and W.F. Rosenbrand. Cyclic and static laboratory tests on Drammen clay. *Journal of the Geotechnical Engineering Division, ASCE*, 106(GT5):499–513, 1980.

[2] A. Niemunis, T. Wichtmann, and T. Triantafyllidis. A high-cycle accumulation model for sand. *Computers and Geotechnics*, 32(4):245–263, 2005.

[3] A. Niemunis, T. Wichtmann, and Th. Triantafyllidis. Long-term deformations in soils due to cyclic loading. In W. Wu and H.S. Yu, editors, *Springer Proceedings in Physics (International Workshop, Vienna)*, volume 106, pages 427–462. Springer, 2005.

[4] A. Niemunis, T. Wichtmann, and Th. Triantafyllidis. On the definition of the fatigue loading for sand. In *International Workshop on Constitutive Modelling - Development, Implementation, Evaluation, and Application, 12-13 January 2007, Hong Kong*, 2007.

[5] A. Niemunis, T. Wichtmann, and Th. Triantafyllidis. Statial stress fluctuations: acoustic evidence and numerical simulations. In *International Symposium on Numerical Models in Geomechanics, 25-27 April 2007, Rhodes, Greece*, 2007.

[6] T. Wichtmann. Explicit accumulation model for non-cohesive soils under cyclic loading. Dissertation, Schriftenreihe des Institutes für Grundbau und Bodenmechanik der Ruhr-Universität Bochum, Heft 38, 2005.

[7] T. Wichtmann, A. Niemunis, and T. Triantafyllidis. FE-Prognose der Setzung von Flachgründungen auf Sand unter zyklischer Belastung. *Bautechnik*, 82(12), 2005.

[8] T. Wichtmann, A. Niemunis, and T. Triantafyllidis. Strain accumulation in sand due to cyclic loading: drained triaxial tests. *Soil Dynamics and Earthquake Engineering*, 25(12):967–979, 2005.

[9] T. Wichtmann, A. Niemunis, and T. Triantafyllidis. Experimental evidence of a unique flow rule of non-cohesive soils under high-cyclic loading. *Acta Geotechnica*, 1(1):59–73, 2006.

[10] T. Wichtmann, A. Niemunis, and T. Triantafyllidis. On the influence of the polarization and the shape of the strain loop on strain accumulation in sand under high-cyclic loading. *Soil Dynamics and Earthquake Engineering*, 27(1):14–28, 2007.

[11] T. Wichtmann, A. Niemunis, and T. Triantafyllidis. Strain accumulation in sand due to cyclic loading: drained cyclic tests with triaxial extension. *Soil Dynamics and Earthquake Engineering*, 27(1):42–48, 2007.